THE JOURNAL OF PHYSICAL CHEMISTRY A
A JOURNAL OF THE AMERICAN CHEMICAL SOCIETY

pubs.acs.org/JPCA

Article

Calculated and Empirical Values of Vibronic Transition Dipole Moments of Reactive Chemical Intermediates for Determination of Concentrations

Ian W. Jones, Jonathan S. Bersson, Jinjun Liu,* Ketan Sharma, Oleg A. Vasilyev, Terry A. Miller,* and John F. Stanton*

Cite This: *J. Phys. Chem. A* 2023, 127, 4670−4681

Read Online

ACCESS | Metrics & More | Article Recommendations | Supporting Information

ABSTRACT: Absorption spectroscopy has long been known as a technique for making molecular concentration measurements and has received enhanced visibility in recent years with the advent of new techniques, like cavity ring-down spectroscopy, that have increased its sensitivity. To apply the method, it is necessary to have a known molecular absorption cross section for the species of interest, which typically is obtained by measurements of a standard sample of known concentration. However, this method fails if the species is highly reactive, and indirect means for attaining the cross section must be employed. The HO_2 and alkyl peroxy radicals are examples of reactive species for which absorption cross sections have been reported. This work explores and describes for these peroxy radicals the details of an alternative approach for obtaining these cross sections using quantum chemistry methods for the calculation of the transition dipole moment upon whose square the cross section depends. Likewise, details are given for obtaining the transition moment from the experimentally measured cross sections of individual rovibronic lines in the near-IR $\tilde{A}-\tilde{X}$ electronic spectrum of HO_2 and the peaks of the rotational contours in the corresponding electronic transitions for the alkyl (methyl, ethyl, and acetyl) peroxy radicals. In the case of the alkyl peroxy radicals, good agreement for the transition moments, ≈20%, is found between the two methods. However, rather surprisingly, the agreement is significantly poorer, ≈40%, for the HO_2 radical. Possible reasons for this disagreement are discussed.

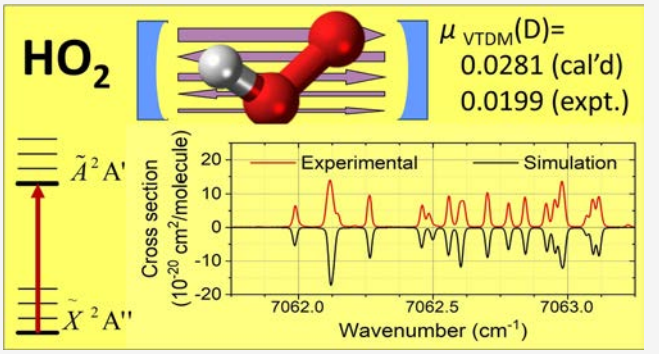

1. INTRODUCTION

Absorption spectroscopy has long been used to measure concentrations, provided the molecule's absorption coefficient is known. For nonreactive molecules, a suitable standard of known concentration/pressure can be used to determine the absorption coefficient, i.e., the product of the molecular absorption cross section and concentration, assuming the path length is measured. However, for many chemical intermediates, such as free radicals, their reactivity precludes preparing such a standard of known concentration, which accounts for the frequent absence of their cross sections in molecular line lists. Nonetheless, such molecules play important roles in chemical reactions of significance both economically and environmentally; hence spectroscopic measurements of their concentrations can be very valuable.

Peroxy radicals, RO_2 (R = H or alkyl group), are intermediates in combustion and tropospheric chemistry and are good examples of reactive chemical intermediates in the gas phase for which rapid and accurate spectroscopic concentration measurements would be very valuable. Indeed, considerable effort has been expended to make such measurements possible using their $\tilde{A}-\tilde{X}$ electronic absorption in the near-infrared (NIR) employing cavity ring-down spectroscopy (CRDS). Specific peroxy radicals for which NIR CRDS spectra have been observed and cross sections measured include hydro[1,2] (HO_2), methyl[3,4] (CH_3O_2), ethyl[5−8] ($CH_3CH_2O_2$), and acetyl[9,10] ($CH_3CH(O)O_2$) peroxy radicals.

The CRDS technique provides a method for measuring the intensity of the absorption at various positions in the spectrum from which a corresponding absorption cross section can be derived, provided that the radical's concentration can be measured independently. Several indirect means for measuring the concentrations have been employed. Often the concentration has been determined by measuring the radical's temporal decay due to its self-destruction chemical reaction with a known rate. Another technique[7,9] is an independent

Received: March 7, 2023
Revised: May 3, 2023
Published: May 22, 2023

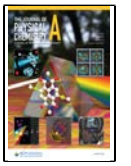

concentration measurement of a nonreactive species (with a known absorption cross section) formed in stoichiometric ratio with the radical.

Experimental absorption cross sections can be obtained from these measurements and then used to measure the concentration of the given species in various other samples. However, care must be taken to ensure that the samples have a common set of physical conditions. Typically, one (or at most a few) spectral line is measured and a Boltzmann equilibrium at a given temperature is assumed to calculate the total population of the species from the measured fraction of molecules in the lower quantum state of the observed transition. Moreover, experimentally only peak cross sections are reported for the peroxy radicals; hence anything, e.g., temperature, total pressure, instrumental resolution, etc., that can modify the spectral line width will affect the measured cross section.

To avoid this limitation, one can assign the quantum states between which the absorption transitions contributing to the measured spectral intensity occur. In principle, such an analysis may be quite challenging particularly since reactive species like peroxy radicals are typically open-shell and have complex fine structure caused by the overall rotation of the molecule and interactions resulting from nonzero electron spin. However, there are now computer programs, e.g., SpecView,[11] PGOPHER,[12] etc., that can aid such an analysis. Indeed, if the molecular fine-structure parameters have been reported from a previous analysis of the electronic absorption spectrum, these programs can reliably simulate the positions of the spectral lines. The intensity of the spectral lines under the conditions for which the experimental cross sections were measured depends additionally upon a measure of the probability that the molecule in the given rovibronic state will absorb a photon at the observed frequency. This probability is specified for the given transition by its vibronic transition dipole moment, VTDM, which can be determined empirically by simulating the spectrum of a sample with a known concentration.

Today it is also possible to calculate the VTDM using quantum chemistry methods. The calculated VTDM can then be combined with the spectral simulation using the molecular constants of the states and at the given experimental conditions. Such an approach does not require an experimentally determined cross section since the spectral simulation with the calculated VTDM provides its value throughout the entire absorption spectrum of a given vibronic band.

The purpose of this paper is to compare for the peroxy radicals mentioned above, VTDM determinations from the experimentally measured cross sections using the PGOPHER software with those calculated using the values of the VTDMs calculated with the CFOUR quantum chemistry suite.[13] The paper's organization is as follows. Section 2 overviews the relationship between the absorption cross section and the corresponding VTDM. In addition it summarizes the calculation of VTDMs using the techniques of quantum chemistry and tabulates calculated values thereof for the various peroxy radicals. In section 3, corresponding empirical values for VTDMs of the individual molecules are determined using the results of section 2. Section 4 compares the resulting values of the VTDMs and provides some general comments about the reliability of each approach. Section 5 summarizes the conclusions of the paper.

2. RELATIONSHIPS AMONG OBSERVED ABSORPTION, MOLECULAR ABSORPTION CROSS SECTION, AND VTDM

2.1. Experimental Determination of VTDMs. Whether performed in an optical cavity or not, the absorbance of a molecular sample can be described by Beer's law,[14]

$$I(\nu) = I_0(\nu)\, e^{-\alpha(\nu)l} \tag{1}$$

where $I_0(\nu)$ and $I(\nu)$ are, respectively, the fluxes of electromagnetic radiation of frequency ν entering and exiting a gas sample of column length l. In conventional absorption spectroscopy, the empirical absorption coefficient $\alpha(\nu)$ can be determined by independently measuring $I(\nu)$ and $I_0(\nu)$, as well as the geometric length of the sample. In a typical CRDS experiment following a pulse of laser light, one measures instead the ring-down times, $\tau_{abs}(\nu)$ and $\tau_{empty}(\nu)$, of an optical cavity of length L, when the absorbing molecular sample of interest is present and absent, respectively. It is well-known[1,2,9] that the absorption coefficient in a CRDS experiment is given by

$$\alpha(\nu) = \frac{L}{lc}\left(\frac{1}{\tau_{abs}} - \frac{1}{\tau_{empty}}\right) \tag{2}$$

where c is the speed of light (see section S.1.1 of the Supporting Information for more details).

It has been conventional in the experimental work on peroxy radicals[1,2,9] to express $\alpha(\nu)$ as a product

$$\alpha(\nu) = \sigma(\nu)N_T \tag{3}$$

where $\sigma(\nu)$ is the cross section for absorption of radiation and N_T is the total number density of sample molecules. One can determine the molecular absorption cross section if one can independently measure $\alpha(\nu)$ and N_T. The total molecular density, or equivalently the concentration, appears in eq 3 because only N_T can be directly measured independently, not the number densities of the particular quantum states involved in the observed transitions. For a nonreactive sample of molecules, N_T can readily be determined by measuring the pressure of the gas in the sample cell. For the case of reactive chemical intermediates like the peroxy radicals, the means of measurement is less direct (and less reliable) and typically involves the measurement of a concentration-dependent property, e.g., the temporal decay rate caused by self-reaction or the concentration of a proxy molecule whose stoichiometric relationship to the radical is known.

Since, as indicated in the Introduction (section 1), $\sigma(\nu)$ depends upon the VTDM, an alternate approach to determining $\sigma(\nu)$ is to calculate the VTDM using quantum chemistry techniques that are detailed in section 3. However, before discussing those details, it is necessary to obtain a relationship between the VTDM for a given molecular transition and the corresponding $\sigma(\nu)$. We discuss this relationship in considerable detail in the Supporting Information and summarize here the most important results. To relate our calculated results of the VTDM to the empirical values of $\sigma(\nu)$, defined by eqs 2 and 3, it is necessary to simulate the observed spectrum. For that task, we use the well-known PGOPHER software,[12] written and documented by Western. In this section and in the Supporting Information, we take care to demonstrate the consistency of the relationships that we obtain and those used in the PGOPHER software.

https://doi.org/10.1021/acs.jpca.3c01584
J. Phys. Chem. A 2023, 127, 4670−4681

In section S.1.2 of the Supporting Information, we see that the cross section, $\sigma^{ul}(\nu)$, for a given spectral transition between upper, u, and lower, l, quantum states can be written as

$$\sigma^{ul}(\nu) = \frac{\pi}{3\varepsilon_0 c\hbar}\nu_{ul}S_{ul}\mathcal{F}_{ul}g(\nu - \nu_{ul}) \tag{4}$$

where ε_0 is the vacuum permittivity, ν_{ul} is the transition frequency, and S_{ul} is the line strength, which is summed over all degenerate magnetic sublevels of both lower and upper states. This equation is equivalent to eq 29 of Western's paper documenting PGOPHER,[12] except that in his equation, the normalized line shape has been integrated over ν to give unity. However, all the reported experimental cross sections for peroxy radicals are peak cross sections, i.e., the maximum value of the cross section at a specified wavenumber, usually ν_{ul}. In that case, subscripts p should be added, giving σ_p^{ul} and $g(\nu - \nu_{ul})_p$.

Physically $\mathcal{F}_{ul}$ is the difference in the number density between the degenerate magnetic sublevels of the quantum states u and l. In sections S.1.2 and S.1.3 of the Supporting Information, we obtain an explicit expression for $\mathcal{F}_{ul}$, valid under the assumption of Boltzmann equilibrium at temperature T and the conditions of the experimental measurements,

$$\mathcal{F}_{ul} = Q_{vib}^{-1}\frac{g_{IJK}\, e^{-E_{IJK}/(k_B T)}}{Q_{rot}} \tag{5}$$

where k_B is the Boltzmann constant and Q_{rot} and Q_{vib} denote, respectively, the rotational and vibrational parts of the molecule's partition function. As discussed in the section S.1 of the Supporting Information, the rotational part of the partition function is provided by the PGOPHER simulation of the rotational, or spin-rotational, structure. The result is that one only needs the calculation of the vibronic partition function, which PGOPHER also can provide. However, some care needs to be exercised since Q_{vib} must include all thermally populated levels of the molecule. This includes vibrational levels giving non-negligible contributions to Q_{vib} even if they are too weakly populated to be observed in the experimental spectrum and low-lying conformers for which independent calculation may be needed. This point is discussed further in section 3 for the individual molecules.

S_{ul} is the molecular line strength function (defined consistently with the atomic line strength).[15] In section S.1.4 of the Supporting Information, we obtain a general expression for S_{ul} appropriate for an asymmetric top molecule

$$S_{ul}(J', K'; J'', K'') = (2J' + 1)(2J'' + 1)\left|\sum_{K'}\sum_{K''} a_{\tau' K'} a_{\tau'' K''}(-1)^{J'-1+K''}\begin{pmatrix} J'' & 1 & J' \\ K'' & K' - K'' & -K' \end{pmatrix}\langle\alpha'\beta'|T^1_{K'-K''}(\mu)|\alpha''\beta''\rangle\right|^2 \tag{6}$$

where $\langle\alpha'\beta'|T^1_{K'-K''}(\mu)|\alpha''\beta''\rangle$ is the VTDM.

The peroxy radicals are all asymmetric tops with rotational eigenvalues $E_{J,\tau}$ and corresponding eigenfunctions that can be expressed as a linear combination of symmetric-top eigenfunctions with coefficients, $a_{J,\tau}$. In addition, most of them are near-prolate symmetric tops, so the symmetric-top quantum number K, while not a good quantum number, is a useful label. In the symmetric-top limit, K becomes a good quantum number, and the general sum over K' and K'' is eliminated, but one still needs to include the degenerate $\pm K$ levels. If the VTDM is set to unity, then for given values of $-K'$ and K'' the RHS of the equation reduces to the normal Hönl−London factor. PGOPHER allows values to be input for the components, either Cartesian or spherical, of the VTDM so that $\sigma_p^{ul}(\nu)$ is calculated.

2.2. Quantum Chemistry Calculations of VTDMs. As we saw in section 2.1, the key molecular property required to obtain the concentration of a species from its electronic absorption spectrum is the VTDM. It can be determined from the experimentally measured cross section, as detailed in section 4, or by calculating its value using quantum chemistry techniques, as is discussed in this section.

For the peroxy radicals considered, we can write a simple equation for the matrix element, M_{vibr}^{AX}, of the VTDM (see eq 6),

$$M_{vibr}^{AX}(v', v'') = G_{v''v'}M_e^{AX} \tag{7}$$

where $G_{v''v'} = \langle v''(q'')|v'(q')\rangle$ is the Franck−Condon overlap (FCO) integral and $M_e^{AX} = \langle\tilde{A}|\hat{\mu}|\tilde{X}\rangle$ is the matrix element of the electric dipole operator $\hat{\mu}$ between the electronic eigenfunctions of the two states involved in the experimentally observed $\tilde{A} \leftarrow \tilde{X}$ transition of the peroxy radicals. We note that to write the VTDM as a simple product as in eq 7, we are assuming that any spin-vibronic mixing of the electronic states is negligible. Since all the experimentally measured absorption coefficients are for transitions that occur between the vibrationless levels of the electronic states, we will often drop the explicit dependence of $M_{vibr}^{AX}(v',v'')$ on v' and v'' unless it is required for distinguishing other vibrational transitions.

To calculate the FCO integral, geometry optimization and normal-mode analysis were performed for the ground and excited states using the UHF-CCSD(T)/aug-pVTZ method with one exception. Since g-$CH_3CH_2O_2$ (the gauche conformer of ethyl peroxy) lacks a plane of symmetry and does not belong to the C_s point group, its $\tilde{A}$ and $\tilde{X}$ states have the same symmetry and therefore the former state cannot be optimized in this manner. For g-$CH_3CH_2O_2$, the $\tilde{A}$ state was optimized using the UHF-EOMEE-CCSD/aug-pVTZ method.

Inputting the results of the calculations into the "FC-squared" ([FC]^2) program available in CFOUR,[16] the FCO overlap integral was obtained as the square root of the outputted Franck−Condon factor (FCF).

Even for the larger RO_2, it is possible to do a calculation for M_e^{AX} at the CCSD(T) optimized geometries using the UHF-EOMEE-CCSD/aug-pVTZ method. However, this calculation lacks both higher-level correlation and residual basis set corrections. There is also a question of the variation of M_e^{AX} with geometry. In order to assess the limitations of this level of calculation for the M_e^{AX} values for the $\tilde{A} \leftarrow \tilde{X}$ transitions of the RO_2 radicals, an extensive series of calculations, which are described in section S.2.2 of the Supporting Information, were performed for the simplest species, HO_2.

It was found that the basis set and correlation errors are modest, each giving scaling factors of slightly more than 0.98, yielding a combined correction factor of $C = 0.96_7$. However, the variation of M_e^{AX} with geometry is more significant. Values calculated at the $\tilde{X}$ and $\tilde{A}$ state optimized geometries vary by ~10% or more (see Table 2). Therefore, M_e^{AX} values were calculated at both geometries and averaged, which should take into account any linear variation of M_e^{AX} with geometry as discussed in section S.2.2.

https://doi.org/10.1021/acs.jpca.3c01584
J. Phys. Chem. A 2023, 127, 4670−4681

The results of our calculations for all the RO_2 radicals are summarized in several tables. Table 1 compares the observed

Table 1. Excitation Energies, $T_{00}(\tilde{A}-\tilde{X})$ (cm^{-1})

	calcd	exptl	rel. error (%)
HO_2	6844	7030	2.6
CH_3O_2	7128	7383	3.5
g-$CH_3CH_2O_2$	7698	7593	1.4
t-$CH_3C(O)O_2$	5554	5583	0.5

$T_{00}(\tilde{A}-\tilde{X})$ excitation energies with those obtained from the CCSD(T) calculations, which include the zero-point-energies determined from the harmonic analysis. The corresponding optimized geometries and rotational constants derived therefrom are provided in section S.2.1 of the Supporting Information. As Table 1 shows, the calculated values agree with the experimentally observed ones to within 4%. Table 2 provides the results of our calculations for the VTDMs and related quantities. The results will be discussed in detail in section 4.

3. EMPIRICAL DETERMINATION OF VTDM FROM OBSERVED ABSORPTION CROSS SECTION

In this section, we turn to the application of the general results of section 2.1 to the determination of VTDMs from the measured cross sections for individual peroxy radicals using the PGOPHER software. The first step is the simulation of the line positions or rotational contours in the peroxy radical spectrum using rotational and spin-rotation constants of the molecule known either from experiment or from quantum chemistry calculations. Alternatively, one can assign the observed spectrum and determine a corresponding set of parameters by least-squares fitting. Fortunately, for all the peroxy radicals, experimental parameter values either exist or can be readily calculated, and these values, at worst, constitute a very good starting place for simulating the spectral line positions, although, for some cases, modest adjustments of these parameters are needed to optimize the simulation of the cross section to match the experimental spectrum.

If a reported cross section can be assigned to a single transition between states u and l, then eq 4 can be directly used to simulate the cross section. The spectrum of HO_2 approximates this situation, as discussed in more detail below. However, for the larger peroxy radicals, only contours containing numerous spin-rotational transitions are observed. Happily, PGOPHER automatically produces a simulation, $\sigma(\nu)$, by summing the cross sections, $\sigma^{ul}(\nu)$, over all u and l states to match the observed contour.

One next has to calculate the fraction, $\mathcal{F}_{ul}$, of the total peroxy radical number density, N_T, that contributes to the intensity at the position of the measured cross section, $\sigma(\nu)$. Eq 5 shows that $\mathcal{F}_{ul}$ depends on the energy of the state l and the partition function Q. The rotational part of Q, Q_{rot}, is automatically incorporated in the PGOPHER simulation. The Supporting Information shows that since all the empirical cross sections are measured for transitions from the vibrationless level, whose energy is taken as zero, $\mathcal{F}_{ul}$ is, to a very good approximation, just the inverse of the vibrational and conformational parts of the partition function. This part of the partition function is readily determined from experimentally observed values and/or ones from quantum chemistry calculations of the vibrational frequencies and relative energies of different conformations in the ground electronic state. Once $\mathcal{F}_{ul}$ is calculated, to obtain the value of the VTDM, it is only necessary to fit its value so that the intensity of the PGOPHER simulation best matches the experimental spectrum.

3.1. The $\tilde{A}^2A'-\tilde{X}^2A''$ Transition of HO_2.

3.1.1. Previous Results. Empirical absorption cross sections were reported by Assaf et al.[2] for the electronic transition $\tilde{A}^2A'(v' = 0)-\tilde{X}^2A''(v'' = 0)$ of HO_2 in a near room-temperature CRDS measurement using a tunable diode laser of narrow bandwidth (≈10 MHz). Under the experimental conditions of 50 Torr He buffer gas, the observed HO_2 line widths averaged 600 MHz due to a combination of pressure and Doppler broadening. Correspondingly, many of the observed lines could be attributed to a single spin-rotational transition with most others being two or three partially overlapped transitions. The Assaf paper reported measurements for the absorption coefficients for 5 such transitions. Conversion of the absorption coefficients to cross sections was accomplished by measurement of the total number density of HO_2 using a previously[1] calibrated $2\nu_1$ rotational transition in the $\tilde{X}$ state, whose density was determined by measuring the HO_2 temporal decay and referencing to the rate constant for its self-reaction.

The first step to obtaining a VTDM for this vibronic transition is to simulate the laser excitation spectrum and

Table 2. Franck–Condon Overlap (FCO) Integrals, Electronic (ETDM) and Vibronic (VTDM) Transition Dipole Moments (D), and Cross Sections (10^{-20} cm^2)

	theory					experiment		
molecule	$\tilde{X}$ ETDM	$\tilde{A}$ ETDM	av. × C	FCO	VTDM	cross section[a]	VTDM[b]	ref
HO_2	0.04175	0.03694	0.03805	0.7375	0.02806	≈10(4)[c]	0.0199(3)	2
CH_3O_2	0.03277	0.04487	0.03753	0.6137	0.02303	4.0(4)	0.0224(15)	3–5
g-$CH_3CH_2O_2$	0.02875	0.03430	0.03048	0.6191	0.01887	0.94(20)[d]	0.0215(8)	6–8
t-$CH_3C(O)O_2$	0.09119	0.08490	0.08805	0.6820	0.05842	10(5)[e]	0.0574(3)	9, 10

[a]Error limits quoted are deduced from those reported by the original experimental works. See section 3.2 for details about the entry for CH_3O_2. [b]Error limits quoted are based on only the statistical uncertainty of the VTDM value from the PGOPHER fits associated with the peak height of the spectrum at a given frequency. These are the corrected values, where necessary, for an incomplete partition function in the PGOPHER calculation (see section 3 for details). Systematic errors are discussed in section 4. [c]Cross-sections for a number of measurements of rotationally resolved transitions, each of which has a unique cross section with a value on the order of 10×10^{-20} cm^2 and the quoted experimental uncertainty. [d]The result given in the table is the average of two consistent, independent values. One value is based on the experimental measurement of ref 7 but corrected for the extended mechanism recommended by ref 8 for determining the molecule's concentration. The other value is an independent measurement in ref 8 of the cross section. [e]Value quoted for the origin transition by ref 9. Ref 10 independently gives a value for a different vibrational transition, which is consistent with this value, based on the experimentally observed transition intensity ratio.

https://doi.org/10.1021/acs.jpca.3c01584
J. Phys. Chem. A 2023, 127, 4670–4681

identify the spin-rotational states involved in these 5 transitions. For the simulation, molecular constants must be identified for the vibrationless level of both the $\tilde{X}$ and $\tilde{A}$ states. The ground electronic ($\tilde{X}^2A''$) state molecular constants of HO_2 were determined by fitting experimentally recorded pure rotational spectra.[17−21] In the present work, we adopt the values reported in ref 21.

Molecular constants for the first excited electronic ($\tilde{A}^2A'$) state of HO_2 were reported by Fink and Ramsay.[22] These authors recorded the FTIR emission spectrum of the origin [(000)−(000)] band of the $\tilde{A}^2A' \rightarrow \tilde{X}^2A''$ transition in the range of 9200−5700 cm^{-1} with a resolution of ≈0.025 cm^{-1}. The excited-state molecular constants are determined from the fitting of the FTIR spectrum (see Table 4 of ref 22).

While PGOPHER predictions of transition frequencies based on these parameters were sufficiently accurate to assign most of the lines for which cross sections had been measured, they were not accurate enough to produce simulations of sufficient fidelity to obtain the best values of the VTDMs. Therefore, we undertook a refitting of the CRD spectrum of HO_2 for this purpose. The details of the refitting, as well as the resulting parameters, are summarized in Table S.4 of the Supporting Information. Using the refit molecular constants, we have obtained spectral simulations of sufficient fidelity, in terms of both line frequencies and *relative* intensities, to reproduce both individual spectral lines and sets of lines from which VTDMs can be extracted. However, before discussing the details of the extraction process, we need to note that using eq 4 for the cross sections contains *two* scaling factors that determine the peak intensity of a given line. These are $\mathcal{F}_{ul}$, given by eq 5, which determines the fraction of the total sample number density that is in the lower state l, and S_{ul}, given by eq 6, which contains the VTDM. As shown in section S.1.3 of the Supporting Information, for the measured empirical cross sections of the peroxy radicals, $\mathcal{F}_{ul}$ reduces to Q_{vib}^{-1}, since Q_{rot}^{-1} is absorbed in the PGOPHER simulation. For HO_2, there is only one conformation, and the lowest vibrational frequency is over 1000 cm^{-1}. Therefore, at Boltzmann equilibrium at near room temperature over 99% of the molecules are in the vibrationless level so that the vibrational part of $\mathcal{F}_{ul}$ can be taken as unity.

3.1.2. Determination of VTDM. We now turn to determining the VTDM from the PGOPHER simulation. Two methods were used in fitting the mostly rotationally resolved line shapes. In the first method (method 1), individual line shapes were fit to the Voigt profile. Approximately one hundred relatively intense and well-resolved peaks in P, Q, and R branches from across the spectrum, were selected for this purpose. The experimental spectrum was comprised of transitions with a maximum J of 30.5. However, the vast majority of the transitions had a J value of 16.5 or less. No specific values of K were selected for method 1. The fit parameters include the transition frequency (ν_0), the Gaussian and Lorentzian line widths (fwhm, $\Delta\nu_G$ and $\Delta\nu_L$), and the VTDM. The rotational and vibrational temperatures were both set to 325 K as determined in ref 2. In the second method (method 2), 5 spectral regions with ≈1.5 cm^{-1} frequency range, each containing five or more transitions were selected. These segments do not contain water absorption lines and have few magnetic dipole transitions. The HO_2 transitions in each segment are mostly fully resolved and include P, Q, and R-branch transitions. The value of the VTDM was fit for all the lines in a given segment with line shapes corresponding to Voigt profiles using the parameters listed in Table 3. Example

Table 3. VTDM and Line Widths (FWHM) Determined in Fitting the Line Shapes in the CRD Spectrum of HO_2[a]

method	VTDM (D)	$\Delta\nu_G$ (cm^{-1})	$\Delta\nu_L$ (cm^{-1})
method 1 (individual peaks)	0.0202(13)	0.0150 (fixed)	0.0032(5)
method 2 (segments)	0.0196(8)		

[a]The numbers in parentheses are one standard deviation (1σ) in the unit of the last digit.

fits of experimental CRD spectra of HO_2 from ref 2 using methods 1 and 2 are illustrated in Figures 1 and 2, respectively. The small systematic errors in fitting the line shapes (see Figures 1a−c) may be attributed to weak transitions of HO_2 or impurities and the collisional narrowing.

In both methods, the molecular constants are fixed to those determined in fit 2 (see Table S.4) except that the vibronic transition frequency (ν_0) was left to float, along with VTDM, $\Delta\nu_G$, and $\Delta\nu_L$. The fit values of $\Delta\nu_G$ using either method are essentially the same as the calculated Doppler broadening of $\Delta\nu_D$ = 0.0150 cm^{-1}. Therefore, the Gaussian contribution to the line width was held fixed to the calculated value of $\Delta\nu_D$ in the final fits of line shapes, while the Lorentzian contribution was fit. The averages and standard deviations of fit values of VTDM, $\Delta\nu_G$, and $\Delta\nu_L$ determined are summarized in Table 3. The fit values for VTDMs from all the methods are about 0.020 D, which should be compared to the calculated value of 0.028 D (see section 2.2 and Table 2).

3.2. The $\tilde{A}^2A'-\tilde{X}^2A''$ Transition of CH_3O_2. The rotational contours of the 0_0^0 origin and 12_1^1 sequence bands (ν_{12} is the internal rotation about the OOCH dihedral angle) of the $\tilde{A}^2A' \leftarrow \tilde{X}^2A''$ transition of the methyl peroxy (CH_3O_2) radical were previously observed[3] in a room-temperature CRDS measurement and are shown in Figure 3. The absorption cross section was obtained using the absorbance determined in the CRDS measurement, the CH_3O_2 concentration, and the absorption length. The CH_3O_2 concentration was calculated using its self-reaction rate and the experimentally measured kinetics of its decay. A value of 2.7×10^{-20} cm^2 was reported for the empirical cross section at the peak of the transition at 7382.8(5) cm^{-1}.[3]

The empirical cross section derived from the spectrum in Figure 3 is the only value directly measured for the origin band of CH_3O_2. However, there are several reports[23−27] of the cross section of the 12_1^1 sequence band that is also shown in Figure 3. In principle the observed spectrum can be used to relate the cross section of the origin to that measured for the sequence band. However, as we discuss below, some uncertainty is introduced by this step. Therefore, we first discuss our analysis of the origin band and then that of the 12_1^1 sequence band.

As is the case for hydro peroxy radical, the first step in the determination of the methyl peroxy VTDM for the 0_0^0 band is the simulation of the experimental spectrum, including both the line positions and relative intensities. To accomplish this requires the rotational and spin-rotation constants for both the $\tilde{A}$ and $\tilde{X}$ states. An early[3] contour fit of the room-temperature spectrum reported rotational constants. However, this fit did not include spin-rotation coupling as it had not been resolved at that time. There are still no experimental spin-rotation coupling constants available for CH_3O_2 because of a lifetime broadening of ≈4 GHz of its spectral lines.[28] Nonetheless,

https://doi.org/10.1021/acs.jpca.3c01584
J. Phys. Chem. A 2023, 127, 4670−4681

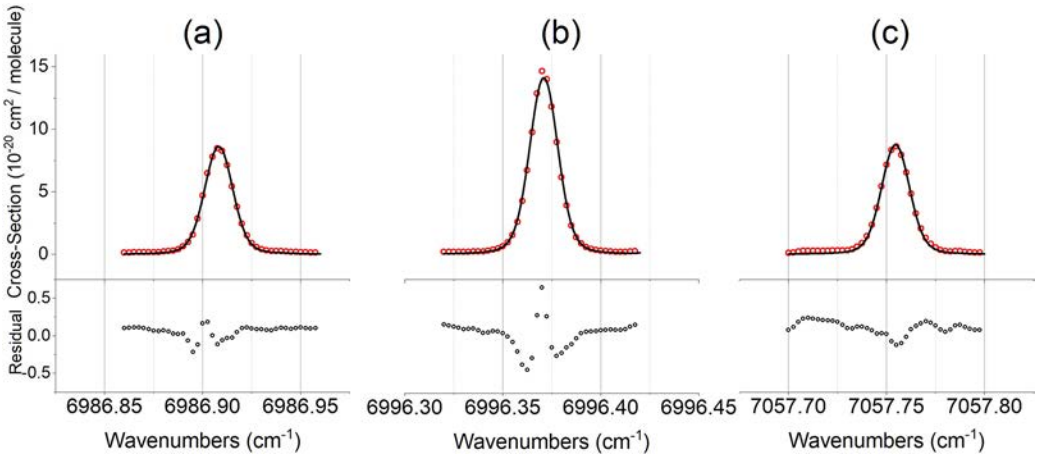

Figure 1. Voigt profile fit of individual P-branch (a), Q-branch (b), and R-branch (c) transitions (black lines) in the $\tilde{A}^2A' \leftarrow \tilde{X}^2A''$ origin band of HO_2 compared to experimental line shapes (red circles) with the residuals of the fit plotted below on an expanded scale. Experimental data from ref 2.

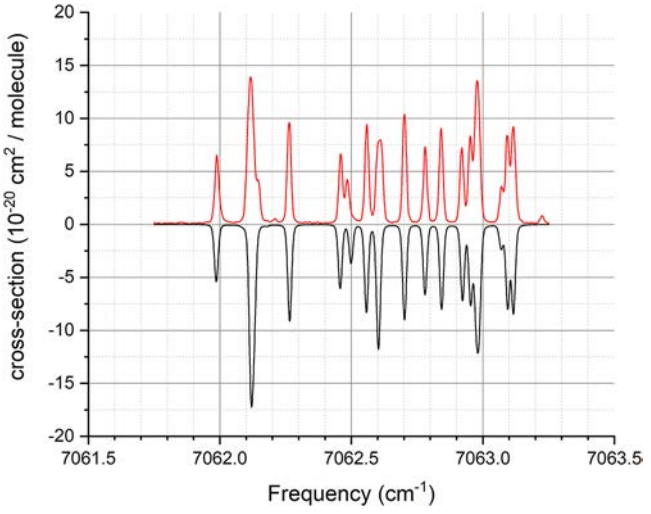

Figure 2. Voigt profile fit of multiple transitions (bottom black) compared to experimental line shapes (top red). Experimental data from ref 2.

there are experimental values of the spin-rotation constants[28] for CD_3O_2, whose spectrum is better resolved. In section S.4 of the Supporting Information, we discuss the appropriate combination of the available data and obtain a set of spin-rotation constants of the methyl peroxy radical.

Using this combination of *ab initio* and semiempirically calculated parameters, the PGOPHER program produces a simulation with a reasonable quality factor of 20, defined as the ratio of the peak intensity to the rms standard deviation of the residuals of the line shape simulation. For the simulation, the rotational and vibrational temperatures are fixed to 300 K. A Voigt profile was used with the FWHMs of both the Gaussian and Lorentzian line shapes fixed to 0.3 cm^{-1}. The Gaussian value is same as that previously reported[3] for the laser bandwidth. The Lorentzian value is discussed below. The spin-rotation constants of the vibrationless levels of the $\tilde{X}$ and $\tilde{A}$ states are fixed to the values calculated from the CD_3O_2 data.

We then fit the rotational contours of the 0_0^0 and 12_1^1 bands simultaneously, allowing the rotational constants and the VTDMs to vary. Figure 3 shows a comparison of the resulting simulation with the experimental trace that contains the origin (0_0^0) band and the first sequence band (12_1^1) of the $\tilde{A} \leftarrow \tilde{X}$ transition of CH_3O_2. The fit values of the parameters are given in Table S.5 in the Supporting Information. Generally speaking, the fit rotational constants are comparable to the calculated ones (to within 8% of the calculated values) and those determined experimentally previously[29] and overall provide a good simulation of the rotational contour. However,

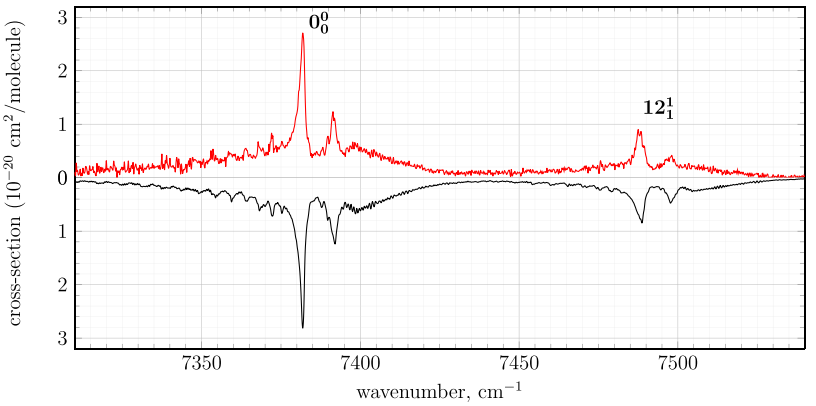

Figure 3. Experimental (top red) and simulated (bottom black) rotational contours of the 0_0^0 and 12_1^1 (higher wavenumber line) bands of the $\tilde{A}^2A' \leftarrow \tilde{X}^2A''$ transition of CH_3O_2. Experimental data and band assignments are from ref 3.

https://doi.org/10.1021/acs.jpca.3c01584
J. Phys. Chem. A 2023, 127, 4670−4681

given the fixing of the spin-rotation constants and the limited information available in the rotational contours, care should be taken regarding their uniqueness and/or physical significance.

The absorption coefficient is determined by the product of $\mathcal{F}_{ul}$ and S_{ul} with the square of the VTDM contained in the latter term. To extract the VTDM, a value for $\mathcal{F}_{ul} = Q^{-1}$ must be calculated. As mentioned earlier for HO_2, the rotational part of the partition function, Q_{rot}, is contained in the rotational simulation in Figure 3. However, unlike HO_2, the vibrational part, Q_{vib}, is not unity but significantly larger for CH_3O_2. This occurs primarily because of its hindered internal rotation, ν_{12}. PGOPHER automatically calculates Q_{vib} for the levels whose transitions are included in the simulation shown in Figure 3, i.e., the vibrationless level and the one with one quantum excited in ν_{12}. This yields a value of $Q_{vib} = 4.64$, which, unfortunately, is not accurate enough, due to neglect of other low-lying vibrational levels that are populated at room temperature. Fortunately, additional levels above $\nu_{12} = 1$ have been well analyzed.[29] To produce a more accurate value of Q_{vib}, we simply sum the ν_{12} energies in that work, including also minor contributions from the COO bend and CO stretch levels below 1000 cm^{-1}. This provides a value of $Q_{vib} = 6.94$, corresponding to a fractional population density in the vibrationless level of 0.144. We then adjust the value of the VTDM, 0.0152 D, found in the PGOPHER fit by the square root of the ratio of the latter Q_{vib} value to the former ($\sqrt{6.94/4.64} = 1.22$) to obtain 0.0184 D for the value of the VTDM.

It is now useful to review the previous measurements of the cross section of the 12_1^1 band. Several of these measurements are by Fittschen and co-workers.[23−26] In these works, CH_3O_2 has been produced by a variety of methods and the cross section determined both using the kinetic method for CH_3O_2 concentration and by calibrating it to that of HO_2, whose cross section had been previously measured. Fittschen[26] nicely summarizes these works in an article in 2019 and argues that the correct value of the cross section for the 12_1^1 transition is 2.2×10^{-20} cm^2.

Concurrent with that work, Onel et al.[27] have reported a value for the 12_1^1 cross section of $1.49(19) \times 10^{-20}$ cm^2. However, it should be noted that the latter value was measured at 7487.98 cm^{-1} compared to the earlier value from the Fittschen group at 7489.16 cm^{-1}. In these experiments, the CH_3O_2 concentration was measured either by the kinetic method or using the "FAGE" (Fluorescence Assay by Gas Expansion) technique.

These 12_1^1 measurements can be used to determine the cross section of the origin band if the ratios of the line intensities at the measured wavelengths are known. The published spectra provide some data on that point; however, it is not entirely consistent. The work of Chung et al.[4] probably provides the best comparison of intensities and leads to a factor of 2.3 to convert the 12_1^1 cross section to a value for the origin. However, the earlier spectrum shown in Figure 3 yields a value of 2.7. Moreover, a PGOPHER simulation, assuming simple Boltzmann equilibrium, finds 1.8, but if the tunneling splitting (see below) is included approximately in the calculation, a value of 2.1 results. Choosing an average value of 2.3(5) for the conversion factor seems appropriate and results in values of $3.4(5) \times 10^{-20}$ cm^2 or $5.1(6) \times 10^{-20}$ cm^2 compared to the directly measured value of $2.7(14) \times 10^{-20}$ cm^2 for the cross section of the origin band.

While not ideal we adopt a simple average of these values, weighted by the inverse squares of their uncertainties, to obtain a cross section value of $4.0(4) \times 10^{-20}$ cm^2 as listed in Table 2. The corresponding derived value of the VTDM therefore increases from 0.0184 D obtained from fitting the data in Figure 3 to a revised value of 0.0221 D, which is also listed in Table 2. Obviously, the reported values of the cross section span a considerable range, but they do overlap within the quoted errors. However, there may be something of a systematic discrepancy between the directly measured values for the 0_0^0 band and the values inferred for it from the measurements on the 12_1^1 band.

Faragó et al.[23] have argued that the cross section for the origin band was underestimated because too high a concentration of CH_3 radicals was produced by the initial laser photolysis in these experiments.[3] This would lead to other radical−radical reactions, in addition to the CH_3O_2 self-reaction, thereby speeding up its decay, causing an overestimation of the CH_3O_2 concentration and a corresponding underestimation of its cross section. While there is good evidence that the proposed mechanism is correct, the estimation used for the initial CH_3 concentration of 5×10^{15} cm^{-3} in the earlier experiments appears to be too high. Zalyubovsky[30] argues that the actual value was in the range of $(0.5−1.5) \times 10^{15}$ cm^{-3}. Using the latter concentration significantly reduces the overestimation of the cross section. Nonetheless, the directly measured value for the origin should probably be taken as a lower limit.

It is worthwhile reminding ourselves of an important fact about peak cross sections. They are strongly dependent on the line width of the observed transition, which is subject to both the intrinsic molecular width and any instrumental broadening, which in this case is caused by the bandwidth of the laser. For the experiments performed by Fittschen and co-workers, the laser bandwidth is negligibly small, ≈0.001 cm^{-1}, as they used narrow-bandwidth diode laser sources. On the other hand, the older cross section value from the Miller group was measured using a tunable pulsed dye laser that is quoted to have a line width of 0.3 cm^{-1}, and the spectrum in Figure 3 was fit with a Voigt profile with 0.3 cm^{-1} for the Gaussian component and 0.3 cm^{-1} for the Lorentzian component. A PGOPHER simulation of the spectrum indicates that if a narrow-bandwidth diode laser were used for the origin measurement it would have increased the experimental peak cross section for the band by 10−20%. However, since the fitting of the laser-broadened spectrum in Figure 3 included the Gaussian width of the laser it should produce a comparable value of the VTDM as would be obtained from fitting an unbroadened spectrum, if it were available.

We should also comment on the quite large Lorentzian contribution to the line width. It may be ascribed to a combination of spectral broadening[28] in the $\tilde{A}$ state of CH_3O_2, probably due to nonradiative transitions, and an unresolved tunneling doublet[4,29] in the $\tilde{X}$ state due to the hindered rotation about the OOCH dihedral angle. These two factors may also play a role in the relatively large discrepancy of the two cross section measurements of the 12_1^1 band. From the published spectra,[23,27] it appears that the larger cross section resulted from fitting a partially resolved peak attributable to a tunneling component, while the smaller value fell between such peaks (see, for example, the spectra in Figure 7 of ref 4).

All of the values of the cross sections quoted above have been measured using the kinetic method for determining the

https://doi.org/10.1021/acs.jpca.3c01584
J. Phys. Chem. A 2023, 127, 4670−4681

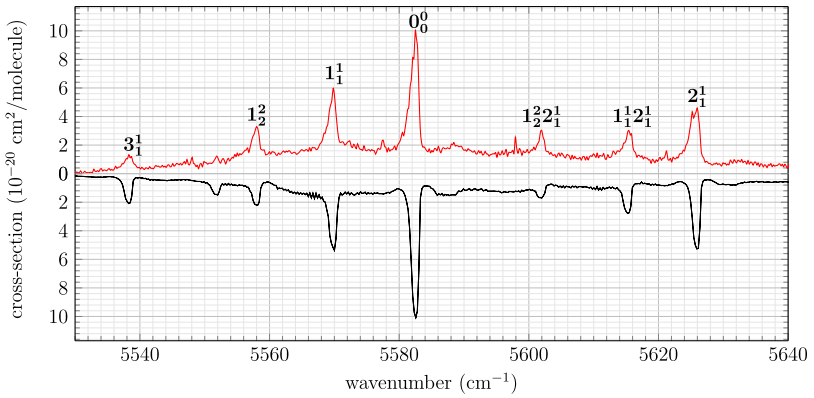

Figure 4. Experimental (top red) and simulated (bottom black) rotational contours of the 0_0^0 (peak intensity) and hot bands of the $\tilde{A}^2A' \leftarrow \tilde{X}^2A''$ transition of *t*-$CH_3C(O)O_2$. Experimental data and band assignments are from ref 9.

CH_3O_2 concentration, either solely or in part. In these reports, the self-reaction rate constant of CH_3O_2 always has been taken near the recommended value[31,32] of $k_{SR} = 3.5 \times 10^{-13}$ cm^3 molecule^{-1} s^{-1} at 298 K (note that because of rapid follow-up reactions the effective, or observed, rate constant, k_{OB}, is 4.8×10^{-13} cm^3 molecule^{-1} s^{-1} for the value of k_{SR} above.) However, a recent report by Onel et al.[33] gives a value of $k_{SR} = 2.1 \times 10^{-13}$ cm^3 molecule^{-1} s^{-1}, 40% lower than the recommended value. Correspondingly, this would lead to a reduction of 40% in the cross sections quoted above. However, the above cross sections are consistent, as is, with measurements of the CH_3O_2 concentration, independent of the CH_3O_2 self-reaction rate, by Fittschen and co-workers.[23,24,26] We therefore choose to list the quoted average from above in Table 2 without modification, pending further investigations of the self-reaction rate constant, k_{SR}.

3.3. Ethyl Peroxy. There have been a number of investigations[6−8,34−36] of the ethyl peroxy radicals by CRDS and several values reported for $\sigma(\nu = 7596\ \text{cm}^{-1})$, where ν is the frequency that has the peak intensity within the $\tilde{A}-\tilde{X}$ origin band. Over the years, reported[37] cross section values have ranged from $(0.3 \text{ to } 1.0) \times 10^{-20}$ cm^2.

The recent work of Zhang et al.[8] has done much to reconcile these varying values, particularly the two most recent ones. Melnik et al.[7] and Zhang et al.[8] have reported σ values of 0.529×10^{-20} and 1.0×10^{-20} cm^2, respectively. Zhang et al. have shown that these two values can be reconciled if the methods for determining the $C_2H_5O_2$ number density are closely examined. Ethyl peroxy radicals were produced by chlorine atom reaction with ethane in both experiments. It was initially assumed that the concentration of $C_2H_5O_2$ was equal to the initial concentration of chlorine atoms. However, chlorine atoms have very fast reactions with $C_2H_5O_2$ and C_2H_5. In the experiments of Melnik et al., these latter reactions constitute a non-negligible loss mechanism; in the experiments of Zhang et al., they are effectively negligible because a much higher ratio of ethane to chlorine atoms was employed. When these losses are included in the reaction mechanism for the Melnick et al. experiments, it is found that the reported cross section should be increased to 8.8×10^{-20} cm^2 well within the experimental error of the value of Zhang et al. We, therefore, use an average of these two values in our calculations, as shown in Table 2.

Unfortunately, the original spectral data are no longer available from the ethyl peroxy CRDS measurement. Therefore, we cannot use PGOPHER to extract a new value of the VTDM. Fortunately, however, that task has already been accomplished,[35] albeit using different software. Since the VTDM is directly proportional to the square root of σ, we can obtain a revised value of VTDM easily. We use the previously reported empirical electronic dipole moment[35] and the Franck−Condon overlap integral from the present work to obtain a value for the VTDM appropriate for that cross section and then multiply it by the square root of the ratio of the revised and old σ's to obtain a revised value for the VTDM of 0.0215 D, the value that appears in Table 2.

3.4. The $\tilde{A}-\tilde{X}$ Transition of Acetyl Peroxy. The $\tilde{A}-\tilde{X}$ transition of acetyl peroxy was recorded in a previous room-temperature CRDS experiment.[9] While numerous vibrational bands were observed, none were rotationally resolved, showing only relatively broad contours. A peak absorption cross section of 1.0×10^{-20} cm^2 at 5582.5 cm^{-1} was measured for the origin band, and its value is given in Table 2. A subsequent investigation of $CH_3C(O)O_2$ by Rolletter et al.[10] has determined the peak cross section for the O−O stretch band at 6510.7 cm^{-1} to be 0.49×10^{-20} cm^2. Since the relative intensities of these two bands differ by about a factor of 2 in the observed spectra, the cross section values are quite consistent. This is particularly pleasing since the measurements of the acetyl peroxy concentrations were done by quite different methods in the two independent experiments.

The $CH_3C(O)O_2$ VTDM was determined in much the same way as for CH_3O_2 (see section 3.2.) The first step is the simulation of the experimental spectrum, including both the line positions and intensities. To accomplish this requires the rotational and spin-rotation constants for both the $\tilde{A}$ and $\tilde{X}$ states. For $CH_3C(O)O_2$, the only source for the rotational constants is based upon the quantum chemistry calculations that we have performed, and these are given in Table S.3 of the Supporting Information. Similarly, estimates of the spin-rotation constants based on those of ethyl peroxy have been obtained and listed in Table S.7 of the Supporting Information. It is assumed that all vibrational levels have the same rotational and spin-rotation constants as the vibrationless level. The VTDM for each vibronic band is assumed equal since all the vibrational bands in Figure 4, except for the origin, are sequence bands. The use of these parameters provides a surprisingly good simulation (T = 300 K, and Gaussian and Lorentzian line widths of 0.1 cm^{-1}) of the experimental spectrum with a quality factor of 21 (see Figure 4). The simulation yields a fit value of 0.0365 D for the VTDM of the origin band.

https://doi.org/10.1021/acs.jpca.3c01584
J. Phys. Chem. A 2023, 127, 4670−4681

However, just as for CH_3O_2, the value of the VTDM must be adjusted because of the incompleteness of the vibrational partition function used by PGOPHER in the simulation. Besides correcting for the population in vibrational levels higher than those that appear in the simulation, acetyl peroxy has two stable conformers, trans (T) and cis (C), defined by the orientation of the OOCO dihedral angle. Our calculations show that the T conformer is 184 cm^{-1} lower in energy than the C conformer (see section S.5). Experimentally, all observed vibronic bands are assigned to the T conformer, but the population of the low-lying C-conformer states must be accounted for in the partition function. We obtain a value of 10.89 for the partition function from the calculation that includes all low-lying levels. Using exactly the same approach as for CH_3O_2, we adjust the PGOPHER VTDM by the square root of the ratio of partition functions ($\sqrt{10.89/3.12} = 1.84$) and obtain the value of 0.0574 D that is listed in Table 2. The vibrational frequencies used in this calculation for each conformer are listed in Table S.8 of the Supporting Information.

4. DISCUSSION

It is enlightening to compare the values of the VTDMs from quantum chemistry calculations and the ones derived from experimental measurements of the absorption cross sections. As Table 2 shows, the agreement between the two sets of results is *very* good in absolute terms. The pairs of values obtained for each molecule agree within 0.01 D. Even in percentage terms, the agreement is still good. For the three alkyl peroxides, the average deviation of the calculated VTDM from the value derived from the experimental cross section is only 6%. The discussion of errors below suggests that this is consistent with the combined uncertainty expected of the calculation and the experimental measurements. For hydro peroxy, the calculated value has a 41% deviation from the experimentally determined one, significantly larger than that for the alkyl peroxy radicals. As will be seen from the discussion below, this may be indicative of a systematic discrepancy between these two results.

Consider first the expected uncertainty of the calculated VTDMs. For all the radicals, the VTDM is a product of two parts, the Franck−Condon overlap integral, FCO, and the electronic transition dipole moment, ETDM. Since HO_2 is the simplest peroxy, it is possible to do vastly more detailed calculations for it than for the alkyl peroxy radicals. As described in section S2.1 of the Supporting Information, in the case of HO_2 for the ETDM it is possible to compute a correction factor of 0.96_7 that accounts for most of the inaccuracies due to the incompleteness of both the basis set and the correlation treatment. However, there still could be a *ca.* 2% residual uncertainty associated with the correction factor.

It was also found that the variation of the ETDM calculated at the $\tilde{A}$ and $\tilde{X}$ state geometries is fairly significant. Taking a simple average of the two values accounts for the linear variation of the ETDM, but higher-order terms in the dipole expansion could still produce an uncertainty of a few percent. The uncertainty of the FCO due to anharmonic effects was assessed by doing a calculation with a quartic force field that produced a value only 1% different from that of the harmonic approximation. A conservative overall uncertainty for the calculated VTDM of HO_2 can be obtained by simply summing the contributions discussed above to yield a value of *ca.* 6%. This value might be expected to rise modestly for the alkyl peroxides, but it seems unlikely that it would be greater than about 10%.

Turning to the experimental VTDMs, it is interesting to note from Table 2, that the uncertainties in the PGOPHER fits are small, always less than 7%. However, as shown in the same table, the corresponding values for the cross section determinations range from 20 to 50%. There are several contributions to these uncertainties. Experimentally it is the absorption coefficient that is measured, which is a product of the total number density, N_T, and the cross section, so N_T must be determined independently to obtain the cross section. For each peroxy radical, N_T has been determined by measuring its rate of destruction by self-reaction using a previously measured rate constant for the reaction, which is termed "the kinetic method". For the two largest radicals, consistent values of the VTDMs have also been found by measuring the assumed stoichiometrically equivalent value of N_T for the HCl formed in the production of HO_2. As these two measurements appear to have comparable errors and the most critical comparison is for HO_2, for which the HCl determination is unavailable, we will restrict further discussion of N_T determinations to those done by the kinetic method.

The kinetic measurements are described in more detail elsewhere.[1,7,8] Generally speaking, they involve measuring the rate of temporal decay of the radicals, which is determined by the product of their initial concentration, N_T, and the self-reaction rate constant k that has previously been measured. N_T must therefore have at least the same percentage error as k. The temporal-decay measurements themselves are not trivial but likely have uncertainties on the order of 10%, in part, since they are sequential, not simultaneous, measurements of (presumed) equivalent samples.

Therefore, the measured rate constants themselves almost always contribute the largest uncertainty to the cross section, ranging up to 40% or more, giving a total experimental uncertainty (square root of sum of squares method) of up to 45% for the cross sections. Since the cross sections depend upon the square of the VTDM, the resulting uncertainty of its value is about 23%. As discussed in section S4.2 of the Supporting Information, uncertainties of (an expected) 10% in the calculated partition function of the alkyl peroxy radicals can cause additional uncertainties up to 5% in the VTDMs. Therefore, based on these considerations we see that for the alkyl peroxides even the maximum deviation of about 13% in Table 2 between the calculated and experimental VTDMs is quite consistent with expectations.

However, the case of HO_2 bears stricter scrutiny. The uncertainties involved in the calculation of its VTDM have been rigorously examined and are relatively small. On the experimental side, all its vibrational frequencies are sufficiently high, assuming Boltzmann equilibrium at near room temperature, that the fraction of molecules in the vibrationless level exceeds 0.99. Hence one can neglect errors in the VTDM from the calculation of the partition function. The kinetic determination of N_T for HO_2 has been quite carefully done, even correcting for minor effects due to the loss of radicals to diffusion processes. The report by Thiebaud et al.[1] convincingly argues that the uncertainty in the cross section from this measurement is 10% or less.

Hence by far the major source of uncertainty is the rate constant, k. In the original papers,[1,2,38] a value of $k = 1.65 \times$

https://doi.org/10.1021/acs.jpca.3c01584
J. Phys. Chem. A 2023, 127, 4670−4681

$10^{-12} + 4 \times 10^{-32}[\mathrm{He}]$ cm^3 molecule^{-1} s^{-1} was used, corresponding to the average at 298 K of the values recommended by the IUPAC[39] and NASA[32] reports. The IUPAC recommendation for its uncertainty is ±40% which gives rise to the uncertainty in the cross section given in Table 2 and a corresponding 20% uncertainty in the empirical VTDM. Therefore, the ≈40% deviation between the calculated and experimental VTDM values is twice what would be expected.

Moreover, two quite recent papers appear to lessen the expected uncertainty of the rate constant significantly. Both theoretical works are quite sophisticated and comprehensive and include the contribution of multiple self-reaction mechanisms, including reaction on both singlet and triplet surfaces and the possibility of adduct formation. The first[40] is a high-level theory paper that includes electronic structure and transition state calculations with a master equation analysis to predict the thermal kinetics of the HO_2 reaction. This work obtained a value of $k = 1.51 \times 10^{-12}$ cm^3 molecule^{-1} s^{-1}. (The quoted value is at 298 K and for 50 Torr N_2 rather than He, but since the pressure dependence of the reaction is slight at this pressure, the difference in the third body should be unimportant.) This value is within 12% of the experimental value (298 K and He as bath gas) quoted above and which was used by Thiebaud et al.[1,2] and Assaf et al.[38] to determine cross sections. The second paper[41] applies multiscale informatics to analyze both the experimental and theoretical data for the self-reaction of HO_2. It predicts a rate constant of $k = 1.71 \times 10^{-12}$ cm^3 molecule^{-1} s^{-1} (298 K and 75 Torr Ar) essentially identical to the experimental value used in the original cross section determination.[1]

However, it should be noted that in the experiments measuring the $\tilde{A}$–$\tilde{X}$ cross section,[2] the reported rotational temperature is actually 325 K, which would lead to about a 15% decrease in the rate constant and cross section. This would lead to a further 7.5% decrease in the VTDM, raising the discrepancy between calculated and experimental values to ≈45%, although in absolute terms, it would still be less than 0.01 D.

We feel that this discrepancy is significant and deserves further investigation. On the experimental side, the most likely source of error not yet considered is the assumption of Boltzmann equilibrium. Since the HO_2 self-reaction is strongly exothermic, it is possible that there is a significant fraction of molecules unrelaxed in otherwise thermally inaccessible vibrational levels of the $\tilde{X}$ state or even the $\tilde{A}$ state. Indeed, the report[2] of a rotational temperature of 325 K for HO_2 in an otherwise ambient temperature gas mixture is an indication of some nonequilibrium behavior in the system, and generally vibrational relaxation is slower than rotational. Such non-equilibrium could lead to a significantly smaller number in the vibrationless level which would then require a larger VTDM to account for the observed cross section. One might question why the assumption of thermal equilibrium would be invalid for HO_2 and not for the other peroxy radicals, for which the calculated VTDMs agree significantly better with the empirically derived values. However, relaxation for the alkyl peroxy radicals may be significantly faster[42] because of the higher density of vibrational levels, particularly those arising from the low-frequency OOCH torsion.

Alternatively, the most obvious possible source of error in the calculated VTDM is the implicit assumption of the validity of the Born–Oppenheimer approximation adopted for calculating the VTDMs. Vibronic interactions are well documented to induce dipole moments on the order of 0.01 D or even greater in other molecules. In an open-shell molecule, electron spin coupling can cause similar effects. Computational investigation of such spin-vibronic effects[43−46] in the $\tilde{A}$–$\tilde{X}$ transition of HO_2 seems warranted.

5. CONCLUSIONS

To determine concentrations by absorption spectroscopy requires knowledge of the cross section for molecular absorption. We have described two methods to obtain the cross section for individual rovibronic transitions using the $\tilde{A}$–$\tilde{X}$ electronic transitions of the hydro and the alkyl peroxy radicals as examples. The first method involves the calculation of the VTDMs using electronic structure methods for the electronic dipole moment and obtaining Franck–Condon vibrational overlap integrals from a calculated harmonic force field. In the second method, the PGOPHER software can be used to obtain VTDM values from experimental cross sections for individual rovibronic lines, including, in some cases, more accurate partition functions than PGOPHER can straightforwardly provide. For all the alkyl peroxy radicals, the VTDMs derived from experimental cross sections disagree less than 15% with those obtained using electronic structure calculations. For HO_2, a larger-than-expected discrepancy of more than 40% is found. Possible reasons for this discrepancy are presented.

■ ASSOCIATED CONTENT

Supporting Information

The Supporting Information is available free of charge at https://pubs.acs.org/doi/10.1021/acs.jpca.3c01584.

Absorption coefficients, cross sections, and vibronic transition dipole moments; Quantum chemistry calculations; Spectroscopic simulation and determination of molecular constants of hydro peroxy; Parameters for methyl peroxy and acetyl peroxy radicals (PDF)

■ AUTHOR INFORMATION

Corresponding Authors

Jinjun Liu − *Department of Chemistry, University of Louisville, Louisville, Kentucky 40292, United States; Department of Physics, University of Louisville, Louisville, Kentucky 40292, United States;* orcid.org/0000-0002-3968-2059; Email: j.liu@louisville.edu

Terry A. Miller − *Department of Chemistry and Biochemistry, The Ohio State University, Columbus, Ohio 43210, United States;* orcid.org/0000-0003-0731-8006; Email: tamiller@chemistry.ohio-state.edu

John F. Stanton − *Departments of Chemistry and Physics, University of Florida, Gainesville, Florida 32611, United States;* orcid.org/0000-0003-2345-9781; Email: johnstanton@chem.ufl.edu

Authors

Ian W. Jones − *Department of Chemistry, University of Louisville, Louisville, Kentucky 40292, United States*

Jonathan S. Bersson − *Department of Chemistry, University of Louisville, Louisville, Kentucky 40292, United States*

Ketan Sharma − *Department of Chemistry and Biochemistry, The Ohio State University, Columbus, Ohio 43210, United States*

https://doi.org/10.1021/acs.jpca.3c01584
J. Phys. Chem. A 2023, 127, 4670−4681

Oleg A. Vasilyev − *Department of Chemistry and Biochemistry, The Ohio State University, Columbus, Ohio 43210, United States;* orcid.org/0000-0002-4678-5603

Complete contact information is available at: https://pubs.acs.org/10.1021/acs.jpca.3c01584

Notes

The authors declare no competing financial interest.

■ ACKNOWLEDGMENTS

The material includes research work supported by NASA Kentucky under NASA award No. 80NSSC20M0047. I.W.J. is supported as a NASA Kentucky Graduate Fellow (Award Nos. GF-21-053 and GF-22-048). J.S.B. was supported through a NSF Research Experiences for Undergraduates (REU) program (Grant No. EEC-2051002). This work was supported by the National Science Foundation under Grant No. CHE-1955310. J.F.S. acknowledges the financial support received from the US Department of Energy, Office of Basic Energy Sciences, under Award DE-SC0018164. O.A.V. gratefully acknowledges a Terry A. Miller Postdoctoral Fellowship from The Ohio State University. T.A.M. acknowledges support from the Ohio Supercomputer via Project No. PAS0540. We thank Christa Fittschen for many helpful discussions, particularly those concerning the cross section for the 12_1^1 transition of CH_3O_2 and her sharing of experimental data for the HO_2 spectrum. We also thank Stephen Klippenstein and Michael Burke, who each provided numerical values for the HO_2 rate constants quoted in the text, and acknowledge helpful discussions with John Barker.

■ REFERENCES

(1) Thiebaud, J.; Crunaire, S.; Fittschen, C. Measurements of Line Strengths in the $2\nu_1$ Band of the HO_2 Radical Using Laser Photolysis/Continuous Wave Cavity Ring-Down Spectroscopy (CW-CRDS). *J. Phys. Chem. A* **2007**, *111*, 6959.

(2) Assaf, E.; Asvany, O.; Votava, O.; Batut, S.; Schoemaecker, C.; Fittschen, C. Measurement of Line Strengths in the $\tilde{A}^2A' \rightarrow \tilde{X}^2A''$ Transition of HO_2 and DO_2. *J. Quant. Spectrosc. Radiat. Transfer* **2017**, *201*, 161−170.

(3) Pushkarsky, M. B.; Zalyubovsky, S. J.; Miller, T. A. Detection and Characterization of Alkyl Peroxy Radicals Using Cavity Ringdown Spectroscopy. *J. Chem. Phys.* **2000**, *112*, 10695.

(4) Chung, C.-Y.; Cheng, C.-W.; Lee, Y.-P.; Liao, H.-Y.; Sharp, E. N.; Rupper, P.; Miller, T. A. Rovibronic Bands of the $\tilde{A} \leftarrow \tilde{X}$ Transition of CH_3OO and CD_3OO Detected with Cavity Ringdown Absorption Near 1.2−1.4 μm. *J. Chem. Phys.* **2007**, *127*, 044311.

(5) Atkinson, D. B.; Spillman, J. L. Alkyl Peroxy Radical Kinetics Measured Using Near-Infrared CW-Cavity Ring-Down Spectroscopy. *J. Phys. Chem. A* **2002**, *106*, 8891.

(6) Rupper, P.; Sharp, E. N.; Tarczay, G.; Miller, T. A. Investigation of Ethyl Peroxy Radical Conformers Via Cavity Ringdown Spectroscopy of the $\tilde{A} - \tilde{X}$ Electronic Transition. *J. Phys. Chem. A* **2007**, *111*, 832.

(7) Melnik, D.; Chhantyal-Pun, R.; Miller, T. A. Measurement of the Absolute Absorption Cross Sections of the $\tilde{A} \leftarrow \tilde{X}$ Transition in Organic Peroxy Radicals by Dual Wavelength Cavity-Ringdown Spectroscopy. *J. Phys. Chem. A* **2010**, *114*, 11583.

(8) Zhang, C.; Shamas, M.; Assali, M.; Tang, X.; Zhang, W.; Pillier, L.; Schoemaecker, C.; Fittschen, C. Absolute Absorption Cross-Section of the $\tilde{A} \leftarrow \tilde{X}$ Electronic Transition of the Ethyl Peroxy Radical and Rate Constant of Its Cross Reaction with HO_2. *Photonics* **2021**, *8*, 296.

(9) Zalyubovsky, S. J.; Glover, B. G.; Miller, T. A. Cavity Ringdown Spectroscopy of the $\tilde{A} - \tilde{X}$ Electronic Transition of the $CH_3C(O)O_2$ Radical. *J. Phys. Chem. A* **2003**, *107*, 7704.

(10) Rolletter, M.; Assaf, E.; Assali, M.; Fuchs, H.; Fittschen, C. The Absorption Spectrum and Absolute Absorption Cross Sections of Acetylperoxy Radicals, $CH_3C(O)O_2$ in the Near IR. *J. Quant. Spectrosc. Radiat. Transfer* **2020**, *245*, 106877.

(11) Stakhursky, V. L.; Miller, T. A. SpecView: Simulation and Fitting of Rotational Structure of Electronic and Vibronic Bands. 56th International Symposium on Molecular Spectroscopy The Ohio State University, Columbus, OH 2001, TC06, https://www.asc.ohio-state.edu/miller.104/molspect/goes/specview.html.

(12) Western, C. M. PGOPHER: A Program for Simulating Rotational, Vibrational and Electronic Spectra. *J. Quant. Spectrosc. Radiat. Transfer* **2017**, *186*, 221−242.

(13) Stanton, J. F.; Gauss, J.; Cheng, L.; Harding, M. E.; Matthews, D. A.; Szalay, P. G. *CFOUR, Coupled-Cluster techniques for Computational Chemistry, a Quantum-Chemical Program Package.* With contributions from A.A. Auer, R.J. Bartlett, U. Benedikt, C. Berger, et al. and the integral packages MOLECULE (J. Almlöf and P.R. Taylor), PROPS (P.R. Taylor), ABACUS (T. Helgaker, H.J. Aa. Jensen, P. Jørgensen, and J. Olsen), and ECP routines by A. V. Mitin and C. van Wüllen. For the current version, see http://www.cfour.de.

(14) Bernath, P. F. *Spectra of Atoms and Molecules*, 2nd ed.; Oxford University Press: New York, NY, 2005.

(15) Condon, E. U.; Shortley, G. H. *Theory of Atomic Spectra*; Cambridge University Press: Cambridge, England, 1935.

(16) Rabidoux, S. M.; Eijkhout, V.; Stanton, J. F. A Highly-Efficient Implementation of the Doktorov Recurrence Equations for Franck−Condon Calculations. *J. Chem. Theory Comput.* **2016**, *12*, 728−739.

(17) Beers, Y.; Howard, C. J. The Microwave Spectrum of HO_2 near 65 GHz. *J. Chem. Phys.* **1975**, *63*, 4212−4216.

(18) Saito, S. Microwave Spectrum of the HO_2 Radical. *J. Mol. Spectrosc.* **1977**, *65*, 229−238.

(19) Charo, A.; De Lucia, F. C. The Millimeter and Submillimeter Spectrum of HO_2: The Effects of Unpaired Electronic Spin in a Light Asymmetric Rotor. *J. Mol. Spectrosc.* **1982**, *94*, 426−436.

(20) Chance, K. V.; Park, K.; Evenson, K. M.; Zink, L. R.; Stroh, F. Far-Infrared Spectrum of HO_2. *J. Mol. Spectrosc.* **1995**, *172*, 407.

(21) Chance, K.; Park, K.; Evenson, K.; Zink, L.; Stroh, F.; Fink, E.; Ramsay, D. Improved Molecular Constants for the Ground State of HO_2. *J. Mol. Spectrosc.* **1997**, *183*, 418.

(22) Fink, E. H.; Ramsay, D. A. High-Resolution Study of the $\tilde{A}^2A' \rightarrow \tilde{X}^2A''$ Transition of HO_2: Analysis of the 000−000 Band. *J. Mol. Spectrosc.* **1997**, *185*, 304.

(23) Faragó, E. P.; Viskolcz, B.; Schoemaecker, C.; Fittschen, C. Absorption Spectrum and Absolute Absorption Cross Sections of CH_3O_2 Radicals and CH_3I Molecules in the Wavelength Range 7473−7497 cm^{-1}. *J. Phys. Chem. A* **2013**, *117*, 12802−12811.

(24) Assaf, E.; Song, B.; Tomas, A.; Schoemaecker, C.; Fittschen, C. Rate Constant of the Reaction between CH_3O_2 Radicals and OH Radicals Revisited. *J. Phys. Chem. A* **2016**, *120*, 8923−8932.

(25) Assaf, E.; Schoemaecker, C.; Vereecken, L.; Fittschen, C. The Reaction of Fluorine Atoms with Methanol: Yield of CH_3O/CH_2OH and Rate Constant of the Reactions $CH_3O + CH_3O$ and $CH_3O + HO_2$. *Phys. Chem. Chem. Phys.* **2018**, *20*, 10660−10670.

(26) Fittschen, C. The Reaction of Peroxy Radicals with OH Radicals. *Chem. Phys. Lett.* **2019**, *725*, 102−108.

(27) Onel, L.; Brennan, A.; Gianella, M.; Hooper, J.; Ng, N.; Hancock, G.; Whalley, L.; Seakins, P. W.; Ritchie, G. A. D.; Heard, D. E. An Intercomparison of CH_3O_2 Measurements by Fluorescence Assay by Gas Expansion and Cavity Ring-Down Spectroscopy within HIRAC (Highly Instrumented Reactor for Atmospheric Chemistry). *Atmospheric Measurement Techniques* **2020**, *13*, 2441−2456.

(28) Wu, S.; Dupré, P.; Rupper, P.; Miller, T. A. The Vibrationless $\tilde{A} \leftarrow \tilde{X}$ Transition of the Jet-Cooled Deuterated Methyl Peroxy Radical CD_3O_2 by Cavity Ringdown Spectroscopy. *J. Chem. Phys.* **2007**, *127*, 224305.

(29) Just, G. M. P.; McCoy, A. B.; Miller, T. A. The Effect of Methyl Rotation on the Electronic Spectrum of the Methyl Peroxy Radical. *J. Chem. Phys.* **2007**, *127*, 044310.
(30) Zalyubosky, S. Near IR Cavity Ringdown Spectroscopy of Peroxy Radicals. Ph.D. thesis, The Ohio State University, 2004.
(31) Atkinson, R.; Baulch, D. L.; Cox, R. A.; Crowley, J. N.; Hampson, R. F.; Hynes, R. G.; Jenkin, M. E.; Rossi, M. J.; Troe, J. IUPAC-Subcommittee Evaluated Kinetic and Photochemical Data for Atmospheric Chemistry: Volume II: Gas-Phase Reactions of Organic Species. *Atmos. Chem. Phys.* **2006**, *6*, 3625−4055.
(32) Burkholder, J. B.; Sander, S. P.; Abbatt, J. P. D.; Barker, J. R.; Cappa, C.; Crounse, J. D.; Dibble, T. S.; Huie, R. E.; Kolb, C. E.; Kurylo, D. et al. *Chemical Kinetics and Photochemical Data for Use in Atmospheric Studies*, Evaluation Number 19. 2022; http://jpldataeval.jpl.nasa.gov/.
(33) Onel, L.; Brennan, A.; Østerstrom, F. F.; Cooke, E.; Whalley, L.; Seakins, P. W.; Heard, D. E. Kinetics and Product Branching Ratio Study of the CH_3O_2 Self-Reaction in the Highly Instrumented Reactor for Atmospheric Chemistry. *J. Phys. Chem. A* **2022**, *126*, 7639−7649.
(34) Just, G. M. P.; Rupper, P.; Miller, T. A.; Meerts, W. L. High-Resolution Cavity Ringdown Spectroscopy of the Jet-Cooled Ethyl Peroxy Radical $C_2H_5O_2$. *J. Chem. Phys.* **2009**, *131*, 184303.
(35) Melnik, D.; Thomas, P. S.; Miller, T. A. The Electronic Transition Moment for the 0_0^0 Band of the $\tilde{A} - \tilde{X}$ Transition in the Ethyl Peroxy Radical. *J. Phys. Chem. A* **2011**, *115*, 13931.
(36) Miller, T. A.; Melnik, D. Kinetic Measurements of the $C_2H_5O_2$ Radical Using Time-resolved CW-CRDS Spectroscopy with a Continuous Source. *J. Chem. Phys.* **2013**, *139*, 094201.
(37) Blanksby, S. J.; Ramond, T. M.; Davico, G. E.; Nimlos, M. R.; Kato, S.; Bierbaum, V. M.; Lineberger, W. C.; Ellison, G. B.; Okumura, M. Negative-Ion Photoelectron Spectroscopy, Gas-Phase Acidity, and Thermochemistry of the Peroxyl Radicals CH_3OO and CH_3CH_2OO. *J. Am. Chem. Soc.* **2001**, *123*, 9585−9596.
(38) Assaf, E.; Liu, L.; Schoemaecker, C.; Fittschen, C. Absorption Spectrum and Absorption Cross Sections of the $2\nu_1$ Band of HO_2 between 20 and 760 Torr Air in the Range 6636 and 6639 cm^{-1}. *J. Quant. Spectrosc. Radiat. Transfer* **2018**, *211*, 107−114.
(39) Atkinson, R.; Baulch, D. L.; Cox, R. A.; Crowley, J. N.; Hampson, R. F.; Hynes, R. G.; Jenkin, M. E.; Rossi, M. J.; Troe, J. Evaluated Kinetic and Photochemical Data for Atmospheric Chemistry: Volume I - Gas-Phase Reactions of O_x, HO_x, NO_x and SO_x Species. *Atmos. Chem. Phys.* **2004**, *4*, 1461−1738.
(40) Klippenstein, S. J.; Sivaramakrishnan, R.; Burke, U.; Somers, K. P.; Curran, H. J.; Cai, L.; Pitsch, H.; Pelucchi, M.; Faravelli, T.; Glarborg, P. $HO_2 + HO_2$: High-Level Theory and the Role of Singlet Channels. *Combust. Flame* **2022**, *243*, 111975.
(41) LaGrotta, C. E.; Meng, Q.; Lei, L.; Barbet, M. C.; Hong, Z.; Burke, M. P. Resolving Discrepancies between State-of-the-Art Theory and Experiment for $HO_2 + HO_2$ via Multiscale Informatics. *J. Phys. Chem. A* **2023**, *127*, 799−816.
(42) Smalley, R. E. Dynamics of Electronically Excited States. *Annu. Rev. Phys. Chem.* **1983**, *34*, 129.
(43) Barckholtz, T.; Miller, T. A. Quantitative Insights About Molecules Exhibiting Jahn-Teller and Related Effects. *Int. Rev. Phys. Chem.* **1998**, *17*, 435.
(44) Paul, A. C.; Sharma, K.; Reza, M. A.; Telfah, H.; Miller, T. A.; Liu, J. Laser-Induced Fluorescence and Dispersed-Fluorescence Spectroscopy of the A^2E-X^2A_1 Transition of Jet-Cooled Calcium Methoxide ($CaOCH_3$) Radicals. *J. Chem. Phys.* **2019**, *151*, 134303.
(45) Sharma, K.; Miller, T. A.; Stanton, J. F. Vibronically Coupled States: Computational Considerations and Characterisation of Vibronic and Rovibronic Spectroscopic Parameters. *Int. Rev. Phys. Chem.* **2021**, *40*, 165−298.
(46) Paul, A. C.; Sharma, K.; Telfah, H.; Miller, T. A.; Liu, J. Electronic Spectroscopy of the $\tilde{A}_1{}^2A''/\tilde{A}_2{}^2A' - \tilde{X}^2A'$ Transitions of Jet-Cooled Calcium Ethoxide Radicals: Vibronic Structure of Alkaline Earth Monoalkoxide Radicals of C_s Symmetry. *J. Chem. Phys.* **2021**, *155*, 024301.

https://doi.org/10.1021/acs.jpca.3c01584
J. Phys. Chem. A 2023, 127, 4670−4681